Volume 2 | Number 1 | 7 January 2014 | Pages 1–210

Journal of Materials Chemistry C

Materials for optical and electronic devices

www.rsc.org/MaterialsC

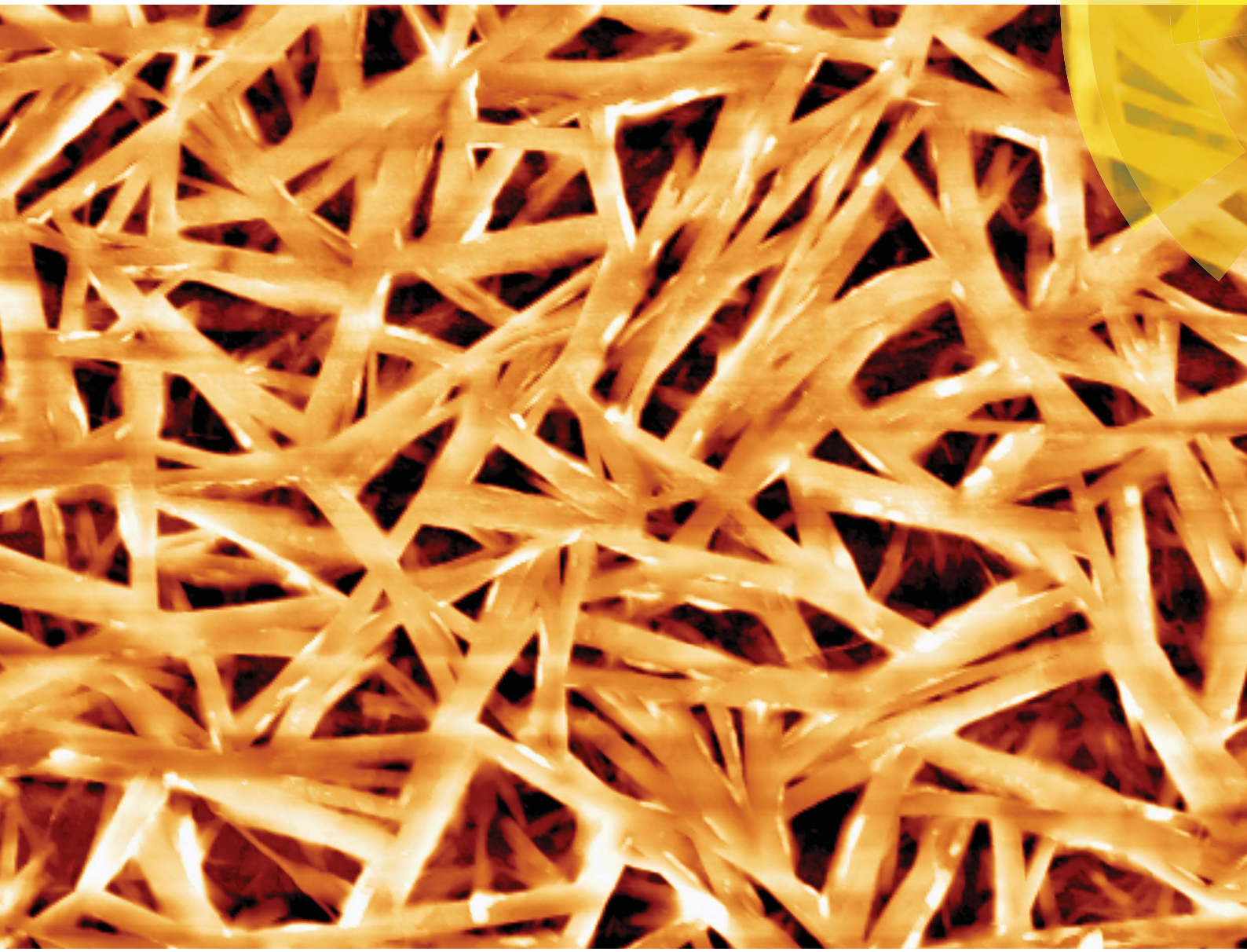

ISSN 2050-7526

ROYAL SOCIETY OF CHEMISTRY

PAPER

Anto R. Inigo, Peter J. Skabara, Ifor D. W. Samuel *et al.*

Charge transport in a two-dimensional molecular organic semiconductor

Journal of Materials Chemistry C

PAPER

View Article Online
View Journal | View Issue

Cite this: J. Mater. Chem. C, 2014, 2, 34

Charge transport in a two-dimensional molecular organic semiconductor†

Sasikumar Arumugam,[a] Iain A. Wright,[a] Anto R. Inigo,*[a] Salvatore Gambino,[bc] Calvyn T. Howells,[b] Alexander L. Kanibolotsky,[a] Peter J. Skabara*[a] and Ifor D. W. Samuel*[b]

Received 26th August 2013
Accepted 19th October 2013

DOI: 10.1039/c3tc31670j

www.rsc.org/MaterialsC

Charge transport has been studied in a germanium-centred oligothiophene cruciform featuring 2-D close packing in the bulk. The morphology has been found to play a significant role in charge carrier transport, evidenced by time-of-flight and field effect transistor measurements. Thermal step-annealing leads to the formation of smaller crystalline domains which are favourable for charge transport in device applications.

Introduction

Increasing the dimensionality of intermolecular interactions in organic semiconducting materials is a promising strategy for improving electronic device performance.[1,2] The most studied multidimensional conjugated systems for organic electronics are based on star-shaped oligomers and dendrimers, which exhibit improved device performance compared to their linear analogues.[3,4] Swivel-type oligothiophene cruciforms were shown to form crystalline films and provide promising materials for field effect transistors.[5] In contrast, rigid spiro-centred cruciform conjugated structures were believed to discourage aggregation and were therefore considered suitable for applications as highly luminescent materials.[6] However, recently we have shown that a Ge spiro-centred oligothiophene cruciform structure (Fig. 1) self-assembles with the formation of efficient π–π stacking in two mutually orthogonal directions yielding a material which can be used as a donor for efficient bulk heterojunction solar cells.[7] In this paper we report mobility measured by time-of-flight and field effect transistor configurations for the **Ge-cruciform**, a semiconducting material with multidirectional intermolecular interactions. We also show that the morphology of the **Ge-cruciform** is greatly affected by post-processing thermal treatment and that this change in morphology can lead to favourable charge transport and improved device performance.

Controlling the morphology of bulk heterojunctions is important for efficient organic photovoltaics.[8–11] The propensity for the **Ge-cruciform** material to crystallise in a 2-D close-packing motif allows us to gain control over the morphology of this material through post-thermal treatment. Here we show for the **Ge-cruciform** that step-annealing leads to the formation of smaller crystalline domains which favour hole transport compared to those annealed directly to the final temperature, where we see the formation of larger crystalline domains which are not favourable for charge transport. We demonstrate how

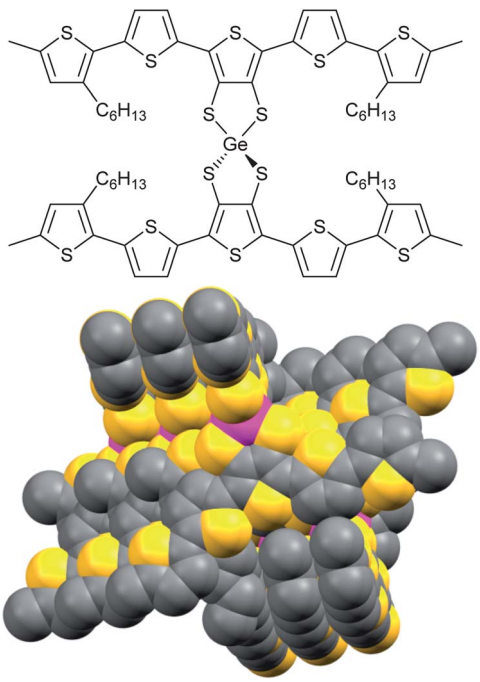

Fig. 1 Structure (top) and packing diagram (bottom) of **Ge-cruciform**, obtained from single-crystal XRD studies.[7]

[a]WestCHEM, Department of Pure and Applied Chemistry, University of Strathclyde, 295, Cathedral Street, Glasgow, G1 1XL, UK. E-mail: anto.inigo@strath.ac.uk; peter.skabara@strath.ac.uk

[b]Organic Semiconductor Centre, SUPA, School of Physics & Astronomy, University of St Andrews, St Andrews, KY16 9SS, UK. E-mail: idws@st-andrews.ac.uk

[c]Centre for Biomolecular Nanotechnologies@UniLe, Istituto Italiano di tecnologia, Via Barsanti, 73010 Arnesano (Le), Italy. E-mail: salvatore.gambino@iit.it

† Electronic supplementary information (ESI) available: Fig. SI1–SI11 as mentioned above. See DOI: 10.1039/c3tc31670j

controlling the morphology of this layer within a planar architecture can alter the performance of a photovoltaic device.

Results and discussion

Field effect transistor mobilities were measured in bottom gate, bottom contact configurations. Field effect transistor characteristics were recorded on as-cast and annealed samples.

Fig. 2 shows the transfer characteristics of two sets of samples with one sample annealed in successive step temperatures of 50, 75, 100 and 120 °C for 20 minutes (data shown for 120 °C), and another sample was annealed straight to 120 °C for 20 minutes. The effect of contact resistances on the output characteristics (Fig. SI1†) of samples annealed straight to 120 °C is stronger than in the case of samples step-annealed to 120 °C. The temperature dependent mobilities of step-annealed samples are shown in Fig. 3 (crossed circles). It can be clearly seen that mobility increases by an order of magnitude moving from 4×10^{-6} cm^2 V^{-1} s^{-1} (unannealed, Fig. SI2†) up to 4×10^{-5} cm^2 V^{-1} s^{-1} after being step-annealed to 120 °C. Meanwhile, the samples annealed straight to 120 °C exhibited much lower mobility, $4 \pm 2 \times 10^{-6}$ cm^2 V^{-1} s^{-1}, compared to that of samples with step-annealing.

Although organic semiconducting materials have been known to exhibit improved performance after annealing closer to their glass transition temperature,[12–14] a large variation in mobility due to step-annealing is very interesting and may play a direct role in the efficiency of, for example, organic photovoltaic (OPV) devices. However, for OPV device applications mobility measurements in the direction perpendicular to the substrate surface are required.[7,15–17] To evaluate this, charge carrier mobilities were also measured using the charge generation layer – time-of-flight (CGL-TOF) method.[18,19] Fig. 4 shows the hole photocurrent transient for an as-cast film on linear and log–log scales (inset), at room temperature and for an applied electric field $E = 3.3 \times 10^4$ V cm^{-1}. The absence of a clear plateau in the photocurrent transient on a linear scale is indicative of highly dispersive charge transport behaviour. In order to estimate the transit time (t_{tr}), a log–log plot was necessary, which allowed measurement of the transit time from the change of slope of the photocurrent transient, $t_{tr} = 43$ μs. The transit time corresponds to a mobility of $\mu = 1 \times 10^{-5}$ cm^2 V^{-1} s^{-1}. We have studied the

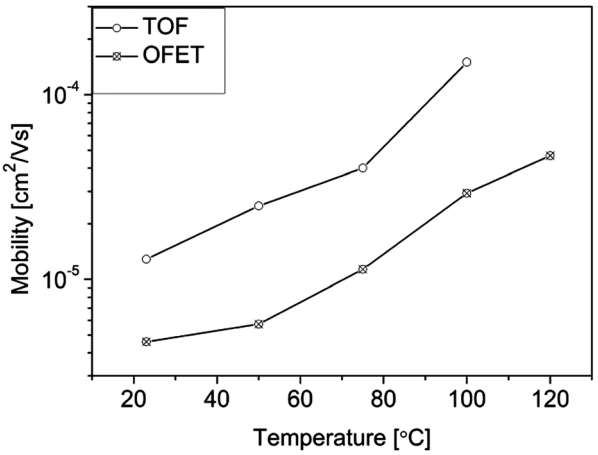

Fig. 3 Temperature dependent mobility of step-annealed **Ge-cruciform** measured by time-of-flight and organic field effect transistor methods.

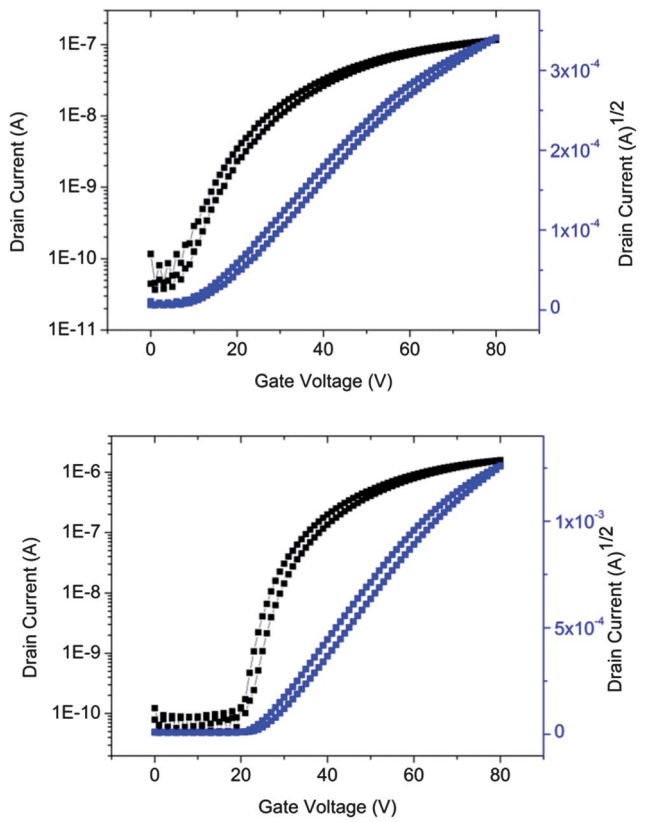

Fig. 2 Transfer characteristics for sample (top) after step-annealing from RT to 120 °C in 20 minutes steps and (bottom) annealed straight to 120 °C for 20 minutes.

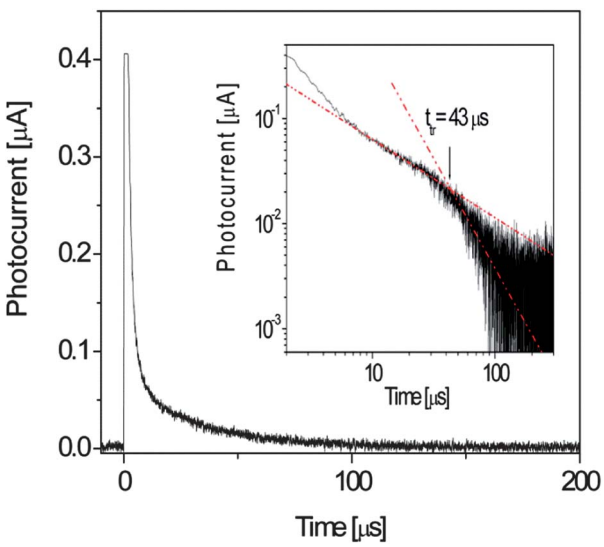

Fig. 4 Hole photocurrent transient on linear and log–log scale (inset) for a film of **Ge-cruciform**, at room temperature and for an applied electric field $E = 3.3 \times 10^4$ V cm^{-1}.

hole mobility field dependence, as shown in Fig. SI4† (squared dots). As the electric field is increased from 3.3×10^4 V cm^{-1} to 3.3×10^5 V cm^{-1}, the hole mobility increases from 1×10^{-5} cm^2 V^{-1} s^{-1} to 3×10^{-5} cm^2 V^{-1} s^{-1}. This field dependent mobility is typical of organic semiconducting materials governed by the Poole–Frenkel relationship with an initial dip and then linear relationship at higher electric fields.[20–23]

Room temperature CGL-TOF measurements were also performed on annealed samples in the same way as for FET mobility (see ESI†). Fig. SI4† shows the hole mobility field dependence for the as-cast sample and the annealed ones at temperatures of 50 and 75 °C. The change in slope (decreasing gradient with increasing temperature) of the field dependent mobility with respect to temperature can be related to the positional disorder present in the material.[19,22,24]

For a direct comparison, Fig. 3 (open circles) shows hole mobility measurements on an as-cast sample and an annealed one at temperatures of 50, 75 and 100 °C. Again, it can be clearly seen that mobility increases by an order of magnitude moving from 1×10^{-5} cm^2 V^{-1} s^{-1}, for the as-cast sample, up to 1×10^{-4} cm^2 V^{-1} s^{-1} for the sample annealed at 100 °C.

It is worth noting here that the charge transport direction in the TOF method is perpendicular to the plane of the substrate, whereas the charge transport direction in OFETs is parallel to the plane of the substrates. While these two different types of measurements are governed by different physical phenomena, for example low level charge carrier density in TOF as opposed to high charge carrier density in OFETs, the general trend of mobility with respect to increase in annealing temperature remains the same. Though one would expect an order of magnitude higher mobility in OFETs than TOF, such differences in absolute mobility values should be accounted by detailed structural morphology with respect to charge transport parameters in the respective charge transport directions since the morphology parameters have larger effects on charge carrier mobility.[25] While these detailed structural and charge transport studies are beyond the scope of this article, the current trend in mobility shown in Fig. 3 with respect to successive annealing temperature indicates that the charge transport pathways in directions parallel and perpendicular to the substrate plane are greatly enhanced by successive annealing and cooling.

Further morphological studies using scanning microscopies support this assumption. Tapping mode AFM height images of as-cast films show that the surface structure is amorphous (Fig. SI5†). In the case of step-annealed samples, crystalline structures start to form around 50 °C. There is no significant difference in the domain or crystalline structures of the samples annealed at temperatures between 50 and 100 °C (Fig. SI5†). However, the rms surface roughness of samples subsequently annealed at 75 and 100 °C is almost double compared to that of samples annealed at 50 °C. This could be due to the reason that crystalline domains start to form above 75 °C, which is further confirmed by independent measurements discussed below. Annealing of the same samples even further at 120 °C for 20 minutes produces broken rod-like crystalline domains of ~200 nm length and 20 nm width (Fig. 5, top).

In the case of samples annealed straight to 120 °C, the tapping mode AFM height images show a nice branching fibrillar structure (Fig. 5, bottom). The structures were of ~10 μm length and ~1 μm width. The horizontal separations between these crystalline rods were as long as 8 μm with random alignment. The random alignment of these bulky rods would be a detrimental factor for observing higher mobilities, since the charge carriers have to overcome rough interfaces in addition to unfavourable alignment of these domains to the direction of the electric field.

Annealing the samples at 120 °C might have given all the molecules relatively similar molecular mobility so that they can form a thermodynamically stable structure, resulting in the long, branching fibrillar structures shown in Fig. 5 (bottom). In

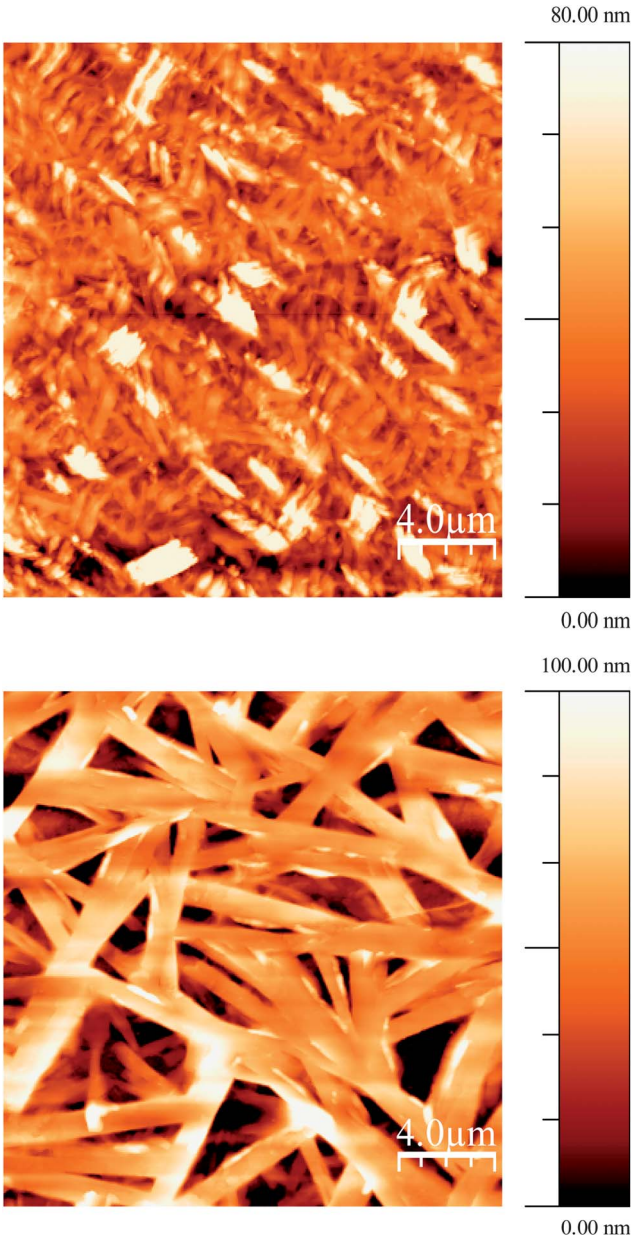

Fig. 5 Tapping mode AFM images of **Ge-cruciform**: (top) annealed at 120 °C for 20 minutes after prior annealing at 50, 75, 100 for 20 minutes; (bottom) annealing straight to 120 °C for 20 minutes.

contrast, successive step-annealing and cooling up to 120 °C might have reduced the molecular mobility due to the formation of smaller crystals at temperatures lower than 100 °C. These observations show that faster annealing promotes growth over the nucleation of crystalline domains; although molecular mobility is important, the rate of nucleation is presumably the dominating factor for the difference in morphologies under these annealing conditions. Once the temperatures are further raised to 120 °C, the crystalline structures already formed at 100 °C may block movements of mobile molecules to form a dense, short-range ordered (DSRO) medium. This type of DSRO medium would be favourable for any type of electronic devices based on charge transport, such as solar cells or OFETs. To demonstrate the effect of post-processing thermal treatment on device performance we fabricated solar cells with a planar heterojunction structure (Fig. 6 top; for energy levels of components, see Fig. SI6†). For this, a low boiling point solvent was required to enable crystals to form at room temperature whilst also drying rapidly to reduce intermixing and allow for crystal growth when annealed straight to 120 °C. For this, carbon disulphide was selected as it previously demonstrated its ability to control cruciform aggregation in bulk heterojunction OPVs.[7] As a comparison, films were also made from the more conventional solvent, chlorobenzene. The films deposited from carbon disulphide or chlorobenzene at room temperature exhibit a similar morphology (Fig. SI7a and SI7c,† respectively). Due to the lower boiling point of carbon disulphide (46 °C), on annealing straight to 120 °C we see the formation of crystalline structures which are rod-shaped (Fig. SI7d†). We observe similar absorption spectra (Fig. SI8†) for films from carbon disulphide or chlorobenzene annealed straight to 120 °C. However, below 450 nm we see some variation due to the size of the structures for films spun from carbon disulphide. Interestingly, we see less structure in absorption for the step-annealed films. Fig. SI9 and SI10† were obtained from a profiler and show the change in morphology between step-annealed and samples annealed straight to 120 °C, respectively. A film of similar thickness was used in the planar devices. Several samples were annealed straight to a given temperature. After acceptor and back electrode deposition they were characterised. A single device that was not annealed was measured at room temperature, then annealed at 50 °C for 20 minutes and measured. The device was subsequently annealed at 75, 100, and 120 °C. Between each temperature ramp of 20 minutes an incident photon to converted electron efficiency (IPCE) measurement was taken. We calculated the short-circuit current density (J_{sc}) under AM1.5G illumination by integrating each IPCE measurement. We see for a single device that step-annealing increases the IPCE (Fig. 7, top), and we observe a sharp fall in IPCE for devices annealed straight to 100 °C or 120 °C (Fig. 7, bottom). When we compare our results by calculating the short-circuit current (Fig. 6), we see similarities with the mobility measurements (Fig. 3). In our studies we see that the morphology of the semiconductor material is greatly influenced by the thermal annealing process and that this change in morphology affects the mobility. Controlling this process through step-annealing allows us to achieve favourable charge transport for improved device performance. For devices annealed directly to 100 or 120 °C we see larger crystalline structures. We show that these structures are unfavourable for charge transport and lead to poor device performance.

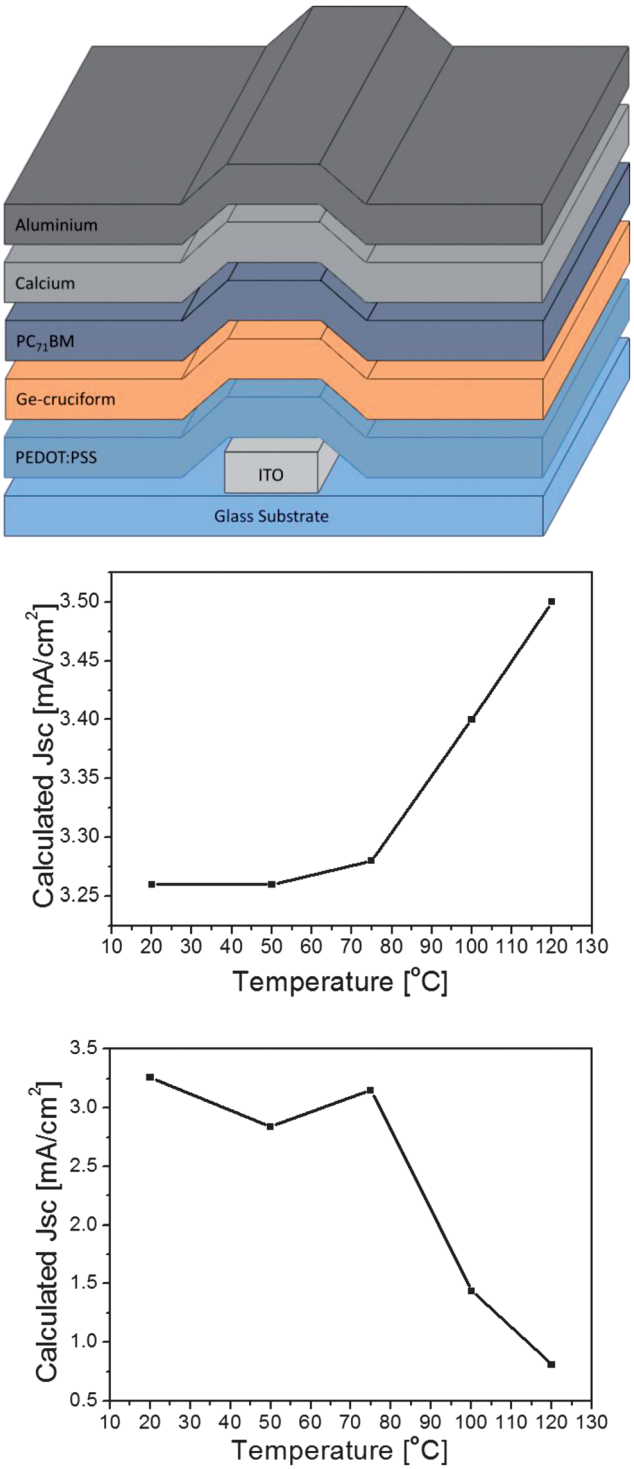

Fig. 6 Device structure of solar cells (top) and short-circuit current calculated for a single device measured at RT, then step-annealed at 50, 75, 100 and 120 °C with measurements taken between each temperature step of 20 minutes (middle) and several individual devices annealed straight to a given temperature for 20 minutes (bottom).

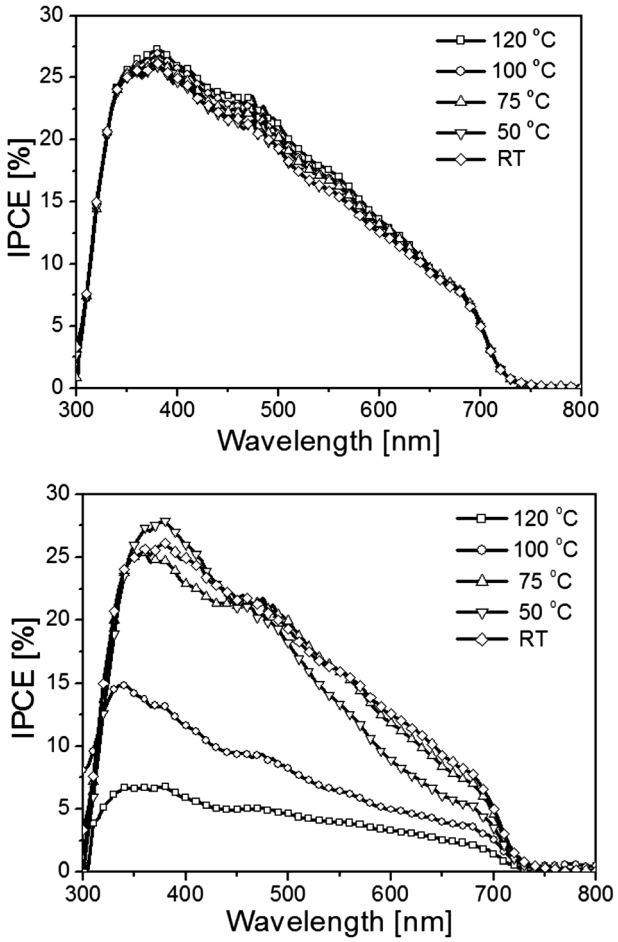

Fig. 7 Top – Single device measured at RT, then annealed at 50 °C for 20 minutes and re-measured. This process was repeated for 75, 100 and 120 °C. An IPCE measurement was taken between each temperature step of 20 minutes. Bottom – IPCE for several devices annealed straight to a given temperature for 20 minutes.

These charge transport measurements on OPV devices, combined with the OFET and TOF results, suggest that the mobilities observed perpendicular to the plane of the substrates by OPV and TOF measurements, and parallel to the plane of substrates by OFET measurements, are influenced by different annealing methods as a function of the material's unique 2-dimensional π–π stacking.

Summary

Temperature dependent mobility of **Ge-cruciform** is measured by using two independent techniques, TOF and OFET, and supports the view that the 2-D stacking interactions favour charge carrier mobility/transport in more than one direction. TOF and OFET carrier mobilities can be enhanced by specific annealing procedures and temperatures to maximise their utilisation in devices such as solar cells and field effect transistors where the charge transport directions are perpendicular to one another. In addition, successive annealing and cooling provided a DSRO medium which was more favourable to charge carrier mobility in the plane of the film and in the orthogonal direction than that of larger crystalline, branching fibrillar structures produced by single annealing. These results highlight the importance of an increase in the bulk dimensionality[1] of organic semiconductors for device performance, which is provided by the 3-D molecular architecture of **Ge-cruciform**.

Experimental

The compound **Ge-cruciform** was synthesised according to the previously reported procedure.[7]

Field effect transistor devices

Organic field effect transistors were fabricated on highly conducting Si with thermally grown 200 nm SiO_2 substrates with prefabricated interdigitated Au fingers with a channel length of 10 μm and channel width of 1 mm. Cleaned substrates were then treated with 10 mM of pentafluorobenzenethiol (PFBT) in ethanol for 15 minutes followed by 10 mM of *n*-octadecyltrichlorosilane (OTS) in toluene for 30 seconds. These treated substrates were then transferred to a nitrogen-controlled MBraun glove box to spin-cast 20 mg/cc solutions of **Ge-cruciform** in chlorobenzene. Current–voltage characteristics were recorded using a Keithley 4200 semiconductor parameter analyser under an air atmosphere. Saturation mobilities were calculated by fitting a straight line to V_{GS} *vs.* $(I_{DS})^{1/2}$ in the saturation region. The surface morphology was investigated by tapping mode atomic force microscopy (AFM), Dimension 3100.

Thermal annealing

One set of samples was annealed at 50, 75, 100 and 120 °C for 20 min in successive order and characterised accordingly. The other set of samples was annealed directly at 120 °C for 20 minutes.

Time-of-flight measurements

For CGL-TOF measurements, solutions of **Ge-cruciform** were made to concentrations of 30 mg ml^{-1} in chlorobenzene. Films were spin-cast onto ITO substrates, in order to obtain a film thickness of around 150 nm. The samples were then transferred to an evaporator where, under high vacuum, a 10 nm layer of the perylene dye (Lumogen Red) was deposited, followed by 100 nm of aluminium. After aluminium deposition the devices were placed in a cryostat where photogeneration of charge carriers in the lumogen red was achieved with a 580 nm pulsed dye laser, which is the peak of the absorption spectrum of Lumogen Red. At this excitation wavelength the **Ge-Cruciform** is transparent (see Fig. SI11†). The aluminium electrode was biased positively and the photocurrent transient detected from the ITO and was recorded using a digital oscilloscope. The devices were then removed from the cryostat and annealed at the required temperature and time before being re-measured. The charge carrier mobility was determined from the transit time (t_{tr}) using the relation:

$$\mu = \frac{L^2}{V \times t_{tr}}$$

where L is the thickness of the organic layer and V is the external applied voltage.

Organic solar cells

Indium tin oxide (ITO) coated glass substrates were masked and etched in hydrochloric acid (37%) for 20 minutes. The mask was removed and the substrates cleaned by sonication in deionised water, acetone and isopropanol. The substrates were dried and placed in an oxygen plasma asher for 5 minutes. Poly(3,4-ethylenedioxythiophene):poly(styrenesulfonate) (PEDOT:PSS) from Clevios (AI4083) was spin-coated on the ITO. The substrates were then placed on a hotplate at 120 °C for 20 minutes in a nitrogen filled glove box. A ~250 nm film of the **Ge-cruciform** was spin-coated from a carbon disulphide solution. Before depositing the acceptor the samples were annealed at a single temperature (either RT, 50, 75, 100 or 120 °C) for 20 minutes. The acceptor [6,6]-phenyl-C_{71}-butyric acid methyl ester ($PC_{71}BM$) from Solenne B. V. Company was spin-coated from a chlorobenzene solution, producing films of ~30 nm. Film thicknesses were measured using a Dektak 150 M stylus profilometer. The samples were then inserted into an evaporator for top electrode deposition. A ~20 nm calcium layer and a ~200 nm aluminium cathode were thermally evaporated at a pressure of 2×10^{-6} mbar. Immediately after electrode deposition the devices were encapsulated with a glass cover slip and a UV activated optical adhesive from Thorlabs. The devices were then removed from the glovebox and characterised in air using an incident photon to charge carrier efficiency (IPCE) setup consisting of an NPL calibrated photodiode, Keithley 6517A picoammeter and a TMc300 monochromator. The device that was not annealed was later annealed at 50, 75, 100 and 120 °C in succession. The annealing time for each temperature was 20 minutes. Incident photon to current efficiency (IPCE) was measured between each temperature ramp. We calculated the short-circuit current density J_{sc} for each IPCE measurement using the equation:

$$J_{sc} = q\int \Phi \times IPCE \mathrm{d}\lambda$$

where:

$$\Phi = \frac{P\lambda}{hc}$$

here P is the AM1.5G spectrum.

For scanning electron microscopy (SEM) and photophysical studies, films were prepared on fused silica substrates from carbon disulphide or chlorobenzene. Samples for OFET, TOF and OPV were produced using the same procedure. SEM images were recorded with a HITACHI S-4800 scanning electron microscope and UV-visible absorption spectra were recorded with a Varian Cary 300 spectrophotometer.

Notes and references

1 P. J. Skabara, J.-B. Arlin and Y. H. Geerts, *Adv. Mater.*, 2013, **25**, 1948.
2 S. Roquet, R. de Bettignies, P. Leriche, A. Cravino and J. Roncali, *J. Mater. Chem.*, 2006, **16**, 3040.
3 A. L. Kanibolotsky, I. F. Perepichka and P. J. Skabara, *Chem. Soc. Rev.*, 2010, **39**, 2695.
4 T. P. I. Saragi, T. Fuhrmann-Lieker and J. Salbeck, *Adv. Funct. Mater.*, 2006, **16**, 966.
5 A. Zen, P. Pingel, F. Jaiser, D. Neher, J. Grenzer, W. Zhuang, J. P. Rabe, A. Bilge, F. Galbrecht, B. S. Nehls, T. Farrell, U. Scherf, R. D. Abellon, F. C. Grozema and L. D. A. Siebbeles, *Chem. Mater.*, 2007, **19**, 1267.
6 J. Pina, J. Seixas de Melo, H. D. Burrows, A. Bilge, T. Farrell, M. Forster and U. Scherf, *J. Phys. Chem. B*, 2006, **110**, 15100.
7 I. A. Wright, A. L. Kanibolotsky, J. Cameron, T. Tuttle, P. J. Skabara, S. J. Coles, C. T. Howells, S. A. J. Thomson, S. Gambino and I. D. W. Samuel, *Angew. Chem., Int. Ed.*, 2012, **51**, 4562.
8 M. T. Dang, L. Hirsch, G. Wantz and J. D. Wuest, *Chem. Rev.*, 2013, **113**, 3734.
9 B. A. Collins, Z. Li, J. R. Tumbleston, E. Gann, C. R. McNeill and H. Ade, *Adv. Energy Mater.*, 2013, **3**, 65.
10 A. J. Moulé and K. Meerholz, *Adv. Mater.*, 2008, **20**, 240.
11 S. J. Lou, J. M. Szarko, T. Xu, L. Yu, T. J. Marks and L. X. Chen, *J. Am. Chem. Soc.*, 2011, **133**, 20661.
12 R. J. Baldwin, T. Kreouzis, M. Shkunov, M. Heeney, W. Zhang and I. McCulloch, *J. Appl. Phys.*, 2007, **101**, 023713.
13 Y. Kim, S. Cook, S. M. Tuladhar, S. A. Choulis, J. Nelson, J. R. Durrant, D. D. C. Bradley, M. Giles, I. McCulloch, C. S. Ha and M. Ree, *Nat. Mater.*, 2006, **5**, 197.
14 C. H. Tan, A. R. Inigo, W. Fann, P.-K. Wei, G.-Y. Perng and S.-A. Chen, *Org. Electron.*, 2002, **3**, 81.
15 D. Cortizo-Lacalle, C. T. Howells, S. Gambino, F. Vilela, Z. Vobecka, N. J. Findlay, A. R. Inigo, S. A. J. Thomson, P. J. Skabara and I. D. W. Samuel, *J. Mater. Chem.*, 2012, **22**, 14119.
16 I. A. Wright, P. J. Skabara, J. C. Forgie, A. L. Kanibolotsky, B. Gonzalez, S. J. Coles, S. Gambino and I. D. W. Samuel, *J. Mater. Chem.*, 2011, **21**, 1462.
17 G. J. McEntee, P. J. Skabara, F. Vilela, S. Tierney, I. D. W. Samuel, S. Gambino, S. J. Coles, M. B. Hursthouse, R. W. Harrington and W. Clegg, *Chem. Mater.*, 2010, **22**, 3000.
18 S. Gambino, A. K. Bansal and I. D. W. Samuel, *Org. Electron.*, 2010, **11**, 467.
19 S. Gambino, S.-C. Lo, Z. Liu, P. L. Burn and I. D. W. Samuel, *Adv. Funct. Mater.*, 2012, **22**, 157.
20 S. Gambino, I. D. W. Samuel, H. Barcena and P. L. Burn, *Org. Electron.*, 2008, **9**, 220.
21 H. Bässler, *Phys. Status Solidi B*, 1993, **175**, 15.
22 S. Gambino, S. G. Stevenson, K. A. Knights, P. L. Burn and I. D. W. Samuel, *Adv. Funct. Mater.*, 2009, **19**, 317.
23 D. Hertel and H. Bässler, *ChemPhysChem*, 2008, **9**, 666.
24 H. Bässler and A. Köhler, in *Unimolecular and Supramolecular Electronics I*, ed. R. M. Metzger, Springer Berlin Heidelberg, 2012, vol. 312, p. 1.
25 Y. F. Huang, C. W. Chang, D. M. Smilgies, U. S. Jeng, A. R. Inigo, J. D. White, K. C. Li, T. S. Lim, T. Li, H. Y. Chen, S. A. Chen, W. C. Chen and W. S. Fann, *Adv. Mater.*, 2009, **21**, 2988.